



Use of iron-crosslinked sodium alginate beads for adsorption of phosphate from solution

Weijiao Pan, Xu Liu*, Peifeng Yang, Runping Han*

College of Chemistry, Zhengzhou University, Kexue Dadao #100, Zhengzhou 450001, China, emails: rphan67@zzu.edu.cn (R. Han), lxcd@zzu.edu.cn (X. Liu), 1792688061@qq.com (W. Pan), 326105497@qq.com (P. Yang)

Received 22 May 2022; Accepted 18 August 2022

ABSTRACT

In this study, Fe-modified sodium alginate (Fe-SA) beads were prepared to enhance the adsorption capacity of SA beads toward phosphate. The adsorbents were characterized by isoelectric point, infrared spectroscopy and X-ray photoelectron spectroscopy. The adsorption characteristics of Fe-SA toward phosphate were presented in batch adsorption. The adsorption conditions of Fe-SA for phosphate ions were optimized, including pH, dose of adsorbent and ionic strength of aqueous solution. The adsorption capacity of Fe-SA to the phosphate can reach $21.3 \text{ mg}\cdot\text{g}^{-1}$ at 293 K. The adsorption behavior of Fe-SA to the phosphate was in line with Temkin model, suggesting that there might be multilayer adsorption in the adsorption process. The mechanism contains chemical adsorption while the adsorption was a spontaneous, entropy-increasing and endothermic process. The spent Fe-SA can be regenerated using $0.1 \text{ mol}\cdot\text{L}^{-1}$ HCl solution. Fe-SA is effective to bind phosphate from solution.

Keywords: Iron modified sodium alginate beads; Adsorption; Phosphate; Regeneration

1. Introduction

Water is considered the most essential component of life. In recent years, with the rapid increase of population and the development of industry, the problem of water shortage and pollution has become increasingly serious. Water may be contaminated by multiple sources of pollution and different types of pollutants, including hazardous chemicals used in human activities, such as fertilizers, industrial wastes, pesticides; Minerals and chemicals in the natural environment, such as arsenic, salt and fluoride; Pollutants that affect taste, smell and color; And pathogens or disease-causing organisms, including bacteria, amoebas and viruses, as well as the eggs and larvae of parasitic worms [1]. Pollution of water systems due to industrialization, climate change, population size and urbanization may increase the likelihood of future freshwater shortages [2].

At present, modern industry uses a large number of synthetic organic compounds to improve product quality, posing toxicity and disease threats to humans and animals. These wastewater contains a large number of harmful organic water pollutants, which are directly released into the water environment and will limit the adequacy of drinking water [3]. Industrial operations such as electrolysis, electroplating and metal smelting can lead to the accumulation of heavy metal ions in wastewater [4]. Water pollution can cause serious harm to human health and ecosystems around the water environment, and wastewater treatment is essential for the recovery of fresh water for human activities and agriculture. Therefore, it is necessary to take reasonable measures to treat sewage [5].

Phosphorus is an essential nutrient element for life activities of living organisms, and is the main component of cell membrane, nucleic acid and skeleton. However,

* Corresponding authors.

excessive intake of phosphorus can lead to loss of calcium in the body and even lead to poisoning. In addition, when the content of phosphorus in water is too high, it will lead to eutrophication in water, resulting in the massive reproduction of algae and other plankton in water and the formation of blooms, which will lead to water pollution, water quality deterioration, the death of fish and other aerobic animals, and the destruction of the original ecological balance [6–8]. The massive propagation of algae and other microorganisms in water reduces the oxygen content and transparency of water, resulting in toxic substances that harm human health [9]. Various anthropogenic wastewater containing phosphorus, such as agricultural wastewater, urban wastewater and some industrial wastewater, can cause eutrophication of water body in a short time. In recent years, water eutrophication is still serious in China, and it frequently occurs in seawater and many fresh water lakes. Therefore, the prevention and control of phosphorus pollution has important practical significance.

Iron-modified nanocellulose, zeolite and IDA can all be used for phosphorus removal. Luo et al. [10] prepared the second generation of iron-supported nanocellulose by loading ferric hydroxide on the natural macromolecule nanocellulose extracted from bamboo, which was used to remove low concentration phosphorus from wastewater. Zhu et al. [11] prepared ferric oxide coated zeolite using natural zeolite and ferric nitrate as raw materials. Iron modification improved the adsorption performance of zeolite, and the removal rate of phosphorus reached more than 80%. Ma et al. modified carbon/zeolite composites (C/ZC) with ferric sulfate, and the maximum adsorption capacity of PO_4^{3-} was $6.94 \text{ mg}\cdot\text{g}^{-1}$, with a removal rate of 99%. Aryee et al. [12] prepared PH- Fe_3O_4 -IDA-Fe and removed phosphate from aqueous solution with a maximum adsorption capacity of $33.7 \text{ mg}\cdot\text{g}^{-1}$ (as P).

Studies show that the acceptable concentration of total phosphorus in the water environment should not exceed $0.03 \text{ mg}\cdot\text{L}^{-1}$ [13]. At present, the most commonly used phosphorus removal methods mainly include chemical precipitation method [14,15], biological method [16–18], ion exchange method [19,20], adsorption method, etc. Among them, adsorption has maintained its popularity among environmental sustainability researchers as a simple, non-toxic, and economical technique. At present, adsorption technology is considered to be the most effective, economical and selective treatment method for sewage purification [19–23]. This method is simple and easy to operate, but different adsorbents have different phosphorus removal efficiency, so the development of new, efficient, green adsorbents is the key to develop a new phosphorus removal process [24–26].

Sodium alginate has been widely used in medicine, fine chemistry, cosmetics, food and other fields due to its good biocompatibility, hygroscopicity, thickening, gelation, stability and degradability [27–30]. Sodium alginate contains a large amount of $-\text{COO}^-$, which can chelate with metal ions in aqueous solution, thus adsorbing metal ions in aqueous solution. Therefore, it is also widely used in the removal of pollutants in water [31,32]. In addition, sodium alginate is non-toxic, green and environmentally friendly. The aim in this study is to prepare iron-crosslinked alginate

beads Fe-modified sodium alginate (Fe-SA) for adsorption of phosphate from solution while the separation of spent Fe-SA from mixtures is easy to be operated. Furthermore, the adsorption capacity is improved after Fe modification. The adsorption kinetics, equilibrium and thermodynamics parameters were studied and desorption of spent Fe-SA were carried out.

2. Materials and methods

2.1. Reagents

The instruments used in this experiment were as follows. The weighing was carried out with an electronic balance (Sartorius BP210S, Germany). The pH value of the solution was measured with a precision pH meter (LeiCi PHS-3C, China) at room temperature. The adsorbent and adsorbent solutions were mixed in a 50 mL conical flask and stirred in a constant temperature shaking bath (GuoHua SHZ-82, China). Electric blast drying oven (YiHeng DHG-9055A, China) was used to dry materials and glassware. The concentration of adsorbent in the aqueous phase was analyzed by UV-vis spectrophotometer (Shunyu Hengping 752, China). Infrared spectra were obtained by Fourier transform infrared spectrometer (PE-1710FTIR, America). Photoelectron spectroscopy was obtained using an X-ray photoelectron spectrometer (Thermo Escalab 250Xi, England).

Sodium alginate (SA), ferric chloride (FeCl_3), potassium dihydrogen phosphate (KH_2PO_4), hydrogen chloride (HCl), sodium hydroxide (NaOH), sodium chloride (NaCl), sodium bicarbonate (NaHCO_3) and other reagents were analytically pure, and the laboratory water was distilled water.

2.2. Preparation of adsorbent

2 g sodium alginate was fully dissolved in 100 mL distilled water, and then the solution was added dropwise into $0.1 \text{ mol}\cdot\text{L}^{-1}$ ferric chloride solution with a dropper. Fe-SA hydrogel spheres were solidified in ferric chloride solution for 8 h, and then oblate spherical Fe-SA hydrogel spheres with diameter of 2–3 mm were obtained. Then the Fe-SA hydrogel spheres were washed with a large amount of distilled water to remove the inorganic ions on the surface of the gel spheres, and placed in distilled water for later use.

2.3. Research methods and content

2.3.1. Adsorption experiment

Adsorption experiments were performed in batch mode. Several factors, such as dosage of adsorbent, adsorption time, initial concentration, solution of the initial solution pH value and temperature are selected to study the effect on adsorption of phosphate. The operation was to take a series of 50 mL conical bottles, including 10 mL phosphate solution and 6 mg Fe-SA (dry weight). The conical bottle was sealed with plastic wrap and oscillated in a thermostatic oscillator for a period of time at a speed of 120 rpm in a constant temperature water bath until the adsorbent was saturated. The adsorbents and adsorbents were separated, and the concentration of phosphate in solution was measured at 700 nm using UV-visible spectrophotometry (molybdenum antimony spectrophotometry).

The adsorption quantity (q_e , $\text{mg}\cdot\text{L}^{-1}$, according to P) and adsorption removal efficiency (p , %) are calculated using Eqs. (1) and (2).

$$q = \frac{V(C_0 - C)}{m} \quad (1)$$

$$p = \frac{(C_0 - C)}{C_0} \times 100\% \quad (2)$$

where m is the mass of adsorbent (g), V is the volume of the adsorbate solution (L), and C_0 and C are the adsorbate concentration in the solution before and after adsorption ($\text{mg}\cdot\text{L}^{-1}$). The experiment was reproducible and each experiment was repeated three times in parallel with average value recorded. The error is less than 5%.

2.3.2. Desorption regeneration

After adsorption ($C_0 = 20 \text{ mg}\cdot\text{L}^{-1}$), the adsorption capacity of q_e ($\text{mg}\cdot\text{g}^{-1}$) was calculated. Then, the spent adsorbent was treated using $0.1 \text{ mol}\cdot\text{L}^{-1}$ HCl solution. Next, the adsorbent was immersed in $0.1 \text{ mol}\cdot\text{L}^{-1}$ FeCl_3 solution (30 min). Then the beads were washed and reused again. The adsorption experimental conditions were consistent with the initial adsorption, and the adsorption capacity q_r ($\text{mg}\cdot\text{g}^{-1}$) of the adsorbent was calculated again. Eqs. (3) and (4) were used to calculate the desorption efficiency (d , %) and regeneration efficiency (r , %), and the optimal desorption method was selected for multiple adsorption-desorption experiments.

$$d = \frac{m_d}{m_0} \times 100\% \quad (3)$$

$$r = \frac{q_r}{q_e} \times 100\% \quad (4)$$

where m_0 is the mass (mg) of adsorbate on the adsorbent and m_d is the mass (mg) of adsorbate desorbed from the adsorbent.

3. Results and discussions

3.1. Characterization of adsorbent

Fourier transform infrared spectroscopy can perform quantitative and qualitative analysis of organic and inorganic samples. FTIR is an effective analytical instrument for detecting functional groups and characterizing information about covalent bonds [33]. Fig. 1a is the infrared spectrum of Fe-SA and SA. The broad absorption peak located at $3,421 \text{ cm}^{-1}$ is due to stretching vibration of $-\text{OH}$, which existed in carboxyl group. Peak at $2,928 \text{ cm}^{-1}$ was due to stretching vibration of $\text{C}-\text{H}$. The peaks located at $1,616$ and $1,416 \text{ cm}^{-1}$ was ascribed to vibration of $\text{O}-\text{C}=\text{O}$. The peak at $1,124 \text{ cm}^{-1}$ was caused by the stretching vibration of $\text{C}-\text{O}-\text{C}$ [34].

It can be seen from Fig. 1a that there is no obvious difference about SA and Fe-SA. The main difference lay in the fingerprint area. Fe-SA has a characteristic absorption peak of $\text{Fe}-\text{O}$ at 587 cm^{-1} , indicating that Fe was successfully connected to SA.

X-ray photoelectron spectroscopy refers to a technique for measuring chemical and elemental state data of the material being analyzed. It is a surface analysis technique that mainly quantifies the thousandth composition, empirical formula, chemical and electronic states of elements present in the sample material. It is widely used in the analysis of polymers, metal alloys, semiconductor, inorganic and biological materials. Fig. 1b showed the photoelectron spectra before and after Fe-SA adsorption. There was peak of $\text{Fe}2p$ from Fe-SA, confirmed Fe-loaded the hydrogel bead. After PO_4^{3-} adsorbed on Fe-SA, two peaks of $\text{Fe}2p$ and $\text{P}2p$ were identified. Furthermore, it was clear that the proportion of $\text{O}1s$ on Fe-SA increased. This implied that the adsorbate be adsorbed on the adsorbent.

3.2. Adsorption study

3.2.1. Effect of pH on adsorption

The effect of pH on the adsorption of PO_4^{3-} by Fe-SA is shown in Fig. 2a. It can be seen from Fig. 2a that when the pH was 3, the adsorption capacity reached the maximum.

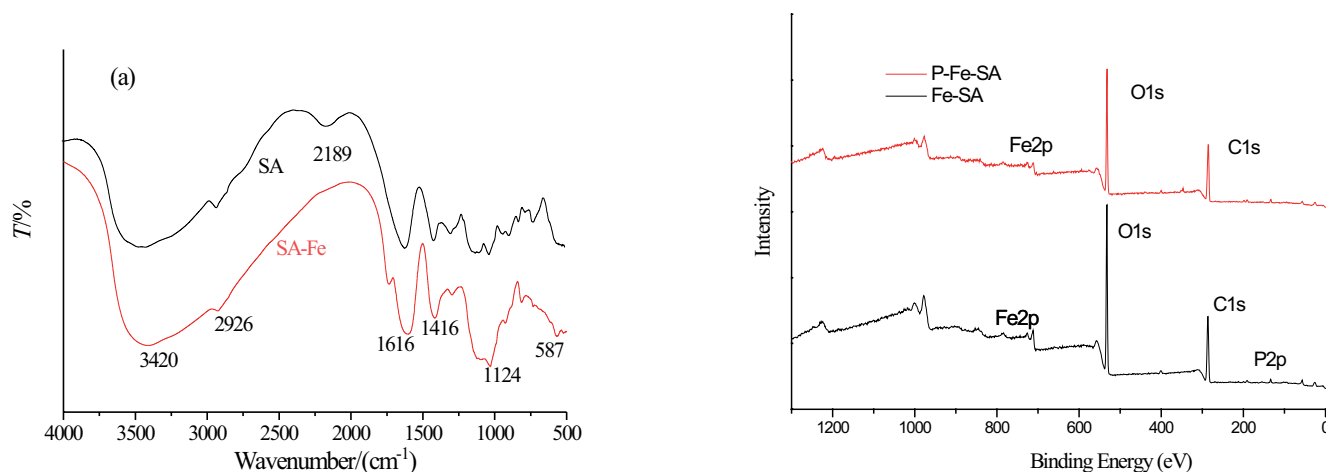


Fig. 1. (a) Infrared spectra of Fe-SA and SA and (b) photoelectron spectra before and after Fe-SA adsorption.

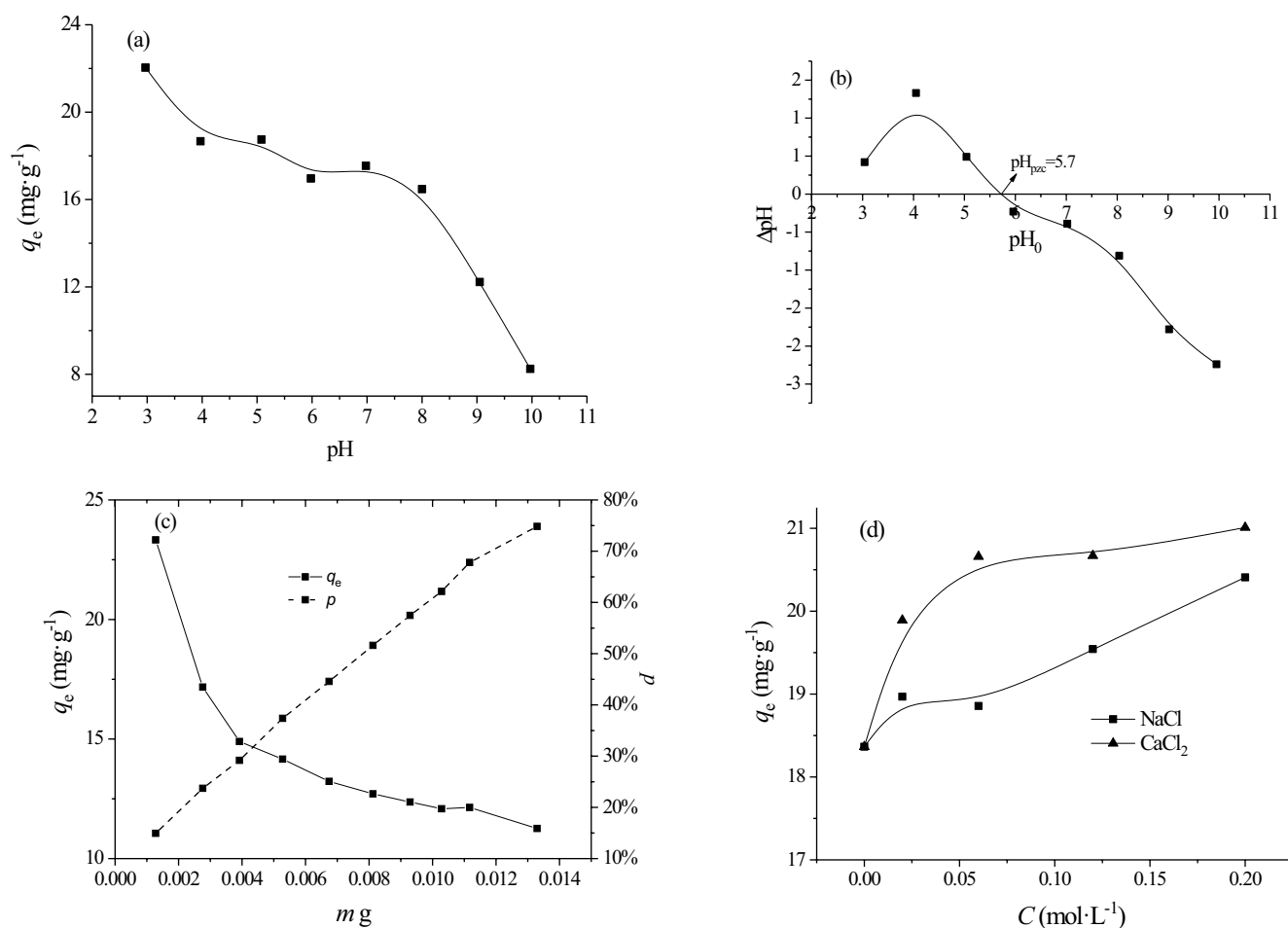


Fig. 2. (a) Effect of pH on adsorption of PO_4^{3-} ($T = 303 \text{ K}$, $C_0 = 20 \text{ mg}\cdot\text{L}^{-1}$, $m = 0.006 \text{ g}$, $t = 4 \text{ h}$), (b) isoelectric point diagrams of Fe-SA ($T = 303 \text{ K}$, $m = 0.01 \text{ g}$, $t = 12 \text{ h}$), (c) effect of adsorbent dosage on Fe-SA adsorption ($T = 303 \text{ K}$, $C_0 = 20 \text{ mg}\cdot\text{L}^{-1}$, $t = 4 \text{ h}$) and (d) effect of salinity on the adsorption ($T = 303 \text{ K}$, $C_0 = 20 \text{ mg}\cdot\text{L}^{-1}$, $m = 0.006 \text{ g}$, $\text{pH} = 3$, $t = 4 \text{ h}$).

As the pH of the solution increased, the adsorption capacity of Fe-SA on PO_4^{3-} gradually decreased. The existing forms of phosphate in different pH solutions include H_3PO_4 , H_2PO_4^- , HPO_4^{2-} , PO_4^{3-} , and their $\text{pK}_{\text{a}1}$, $\text{pK}_{\text{a}2}$, and $\text{pK}_{\text{a}3}$ are 2.13, 7.20, and 12.33, respectively.

The isoelectric point diagram of Fe-SA is shown in Fig. 2b. It can be seen from Fig. 2b that the isoelectric point pH_{pzc} of Fe-SA hydrogel spheres is 5.7. When the pH value of the adsorbate solution was less than the isoelectric point pH_{pzc} of the adsorbent, the surface of the adsorbent was positively charged; when the pH value of the adsorbent solution was greater than the isoelectric point pH_{pzc} , the surface of the adsorbent was negatively charged.

Combined with isoelectric point analysis, when the pH value of the PO_4^{3-} solution was between 3 and 5.7, the adsorbent had a positive surface charge, and the main form of phosphate in the solution was H_2PO_4^- , both of them can be combined by electrostatic attraction and complexation. Therefore, when the pH was greater than 5.7, the surface of the adsorbent was negatively charged, and PO_4^{3-} in the solution mainly existed in the form of negatively charged ions, which can only be adsorbed by complexation, and cannot be adsorbed by electrostatic attraction. On the other

hand, as the pH of the solution increased, the concentration of OH^- ions in the solution increased, and its coordination ability with Fe^{3+} was stronger than that of phosphate and ferric iron. Therefore, the adsorption capacity of Fe-SA to PO_4^{3-} gradually decreased with the increase of solution pH.

At same experimental conditions, there was almost adsorption capacity about hydrogel bead of Ca-SA toward phosphate. This confirmed the role of Fe in SA beads for removal of phosphate.

3.2.2. Influence of the amount of adsorbent on adsorption

The effect of adsorbent dosage on Fe-SA adsorption of PO_4^{3-} is shown in Fig. 2c. It can be seen from Fig. 2c that the adsorption amount of PO_4^{3-} was inversely proportional to the amount of Fe-SA, and proportional to the removal efficiency (p). As the amount of adsorbent increased from 0.001 g to 0.014 g, values of q_e decreased from 23.3 to 11.3 mg·g⁻¹, and p increased from 14.9% to 74.8%. This was because the more Fe-SA was used, the more active sites would be combined with PO_4^{3-} , and the greater the probability of being adsorbed. Therefore, the removal rate would increase. However, when the amount of PO_4^{3-} was

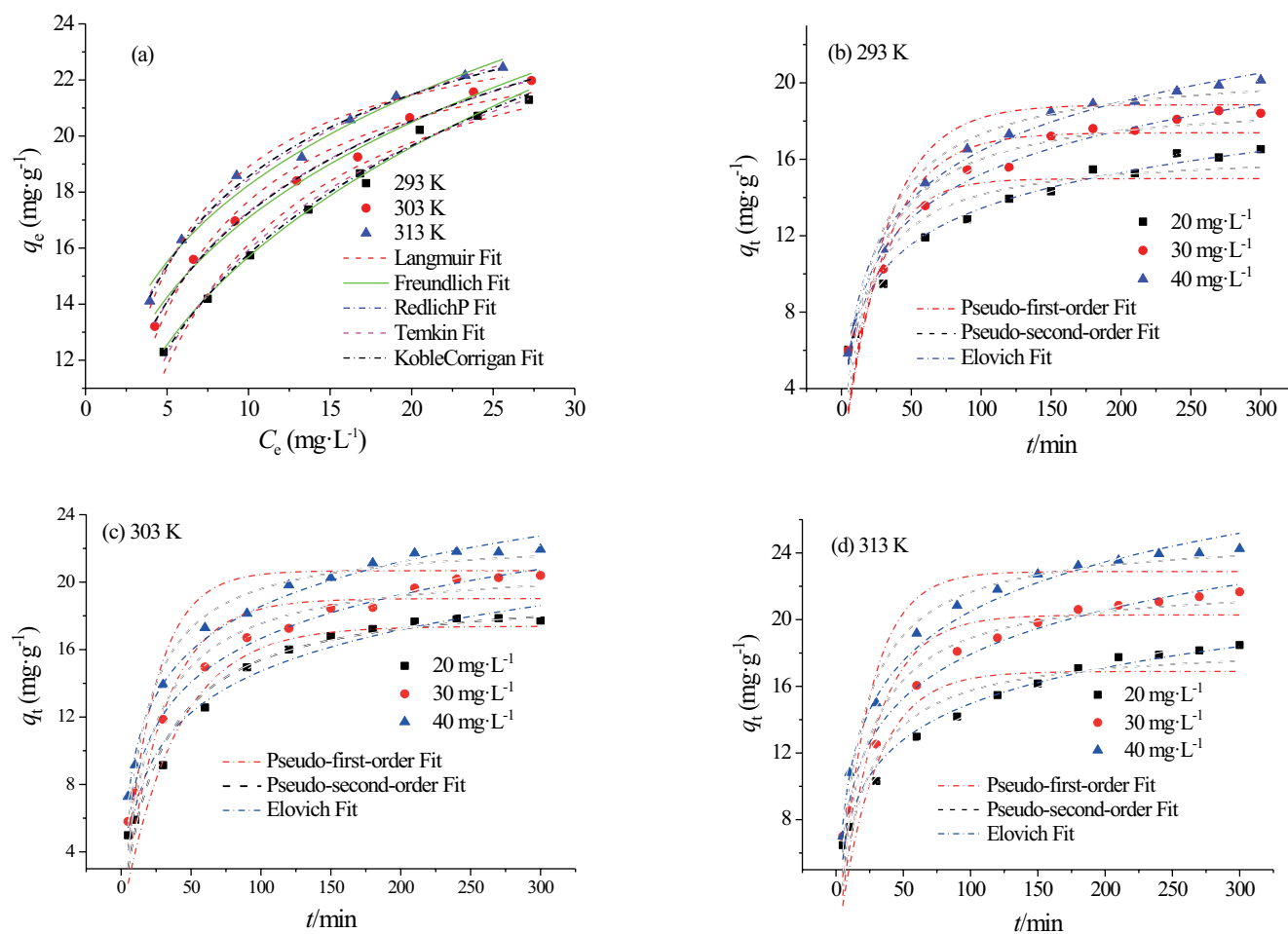


Fig. 3. (a) Effect of concentration of PO_4^{3-} on adsorption and non-linear fitting curves of isotherm ($m = 0.006 \text{ g}$, $t = 4 \text{ h}$, $\text{pH} = 3$); Kinetic curves and non-linear fitting curves of adsorption (b) 293 K, (c) 303 K and (d) 313 K ($m = 0.006 \text{ g}$, $t = 4 \text{ h}$, $\text{pH} = 3$).

constant, the more Fe-SA was used, the less the amount of PO_4^{3-} was evenly distributed to each adsorbent, so the q_e was lowered. Considering the full utilization of the adsorbent and the experimental cost, the dosage of Fe-SA was selected as $0.6 \text{ g}\cdot\text{L}^{-1}$.

3.2.3. Effect of salinity on adsorption

The effect of salinity on the adsorption of PO_4^{3-} by Fe-SA is shown in Fig. 2d. It can be seen from Fig. 2d that the presence of salt ions in the solution was beneficial to the adsorption of PO_4^{3-} on Fe-SA. With the increase of the concentration of NaCl and CaCl_2 in the solution, the adsorption capacity of Fe-SA on PO_4^{3-} increased from 18.4 to 20.4 and $21.0 \text{ mg}\cdot\text{g}^{-1}$, respectively. The degree of increase was small. The effect of CaCl_2 on the adsorption was greater than that of NaCl, which might be because CaCl_2 increased the ionic strength in the solution with greater amplitude and had a greater impact on the electric double layer. This result was similar to many studies on modified adsorbents. The research results showed that the increase in ionic strength increased the adsorption capacity of the adsorbent to the adsorbate, mainly due to the formation of an inner coordination between the adsorbent and the phosphate. Considering the

effects of pH and salinity, it can be inferred that the adsorption process of PO_4^{3-} on Fe-SA might be dominated by the coordination role. Of course, there are also van der Waals forces and hydrogen bonds between phosphate and Fe-SA.

3.2.4. Effect of equilibrium concentration and temperature on adsorption

The effect of phosphate concentration on adsorption is depicted in Fig. 3a. It can be seen from Fig. 3a that at the same temperature, the adsorption capacity of Fe-SA increased with the increase of PO_4^{3-} concentration and temperature. The equilibrium adsorption capacities of Fe-SA for PO_4^{3-} at 293, 303 and 313 K were to 21.3 , 22.0 and $22.4 \text{ mg}\cdot\text{g}^{-1}$, respectively. This may be due to the increased temperature, which made it easier for PO_4^{3-} to enter the inside of Fe-SA, adding new active sites. It showed that the adsorption of Fe-SA to PO_4^{3-} was an endothermic reaction.

Langmuir, Freundlich, Redlich–Peterson, Koble–Corrigan and Temkin models were used to perform isotherm non-linear fitting for Fe-SA adsorption of PO_4^{3-} . Non-linear regressive analysis is performed to obtain the parameters of models and determined coefficient according to least sum of the square of errors (SSE). The expressions of these

Table 1
Adsorption kinetics models used in the study

Model	Equation	Parameters
Isotherm model		
Langmuir model	$q_e = \frac{q_m K_L C_e}{1 + K_L C_e}$	q_e is the equilibrium adsorption quantity ($\text{mg}\cdot\text{g}^{-1}$), C_e is the A_R concentration at equilibrium ($\text{mg}\cdot\text{L}^{-1}$), K_L is the Langmuir binding constant related to the free energy of adsorption ($\text{L}\cdot\text{mg}^{-1}$), q_m is the maximum adsorption capacity ($\text{mg}\cdot\text{g}^{-1}$) [35]
Freundlich model	$q_e = K_F C_e^{1/n}$	K_F and $1/n$ are the Freundlich constants characteristics of the system, implying the adsorption capacity and the adsorption intensity [6]
Redlich–Peterson model	$q_e = \frac{AC_e}{1 + BC_e^g}$	A , B and g are the Redlich–Peterson parameters, g means the degree of heterogeneity, between 0 and 1. If the value of g is 1, the equation is equal to Langmuir [8]
Temkin	$q_e = A + B \ln C_e$	A and B are parameters of Temkin model
Koble–Corrigan	$q_e = \frac{AC_e^n}{1 + BC_e^n}$	A , B and n are parameters of model
Kinetic model		
Pseudo-first-order kinetic model	$q_t = q_e (1 - e^{-k_1 t})$	q_e is the equilibrium adsorption quantity ($\text{mg}\cdot\text{g}^{-1}$) and k_1 is the rate constant of the equation (min^{-1})
Pseudo-second-order kinetic model	$q_t = \frac{k_2 q_e^2 t}{1 + k_2 q_e t}$	k_2 is the rate constant of the equation ($\text{g}\cdot\text{mg}^{-1}\cdot\text{min}^{-1}$)
Elovich equation	$q_t = \frac{\ln(\alpha\beta)}{\beta} + \frac{\ln t}{\beta}$	a is the initial adsorption rate constant ($\text{mg}\cdot\text{g}^{-1}\cdot\text{min}^{-1}$); β is related to the extent of surface coverage and activation energy for chemisorption ($\text{g}\cdot\text{mg}^{-1}$)

models are listed in Table 1. The fitted curves are also shown in Fig. 3a, and the fitting parameters are shown in Table 2.

The Temkin model is mostly used for multi-phase surface adsorption. It can be seen from the table that the value of A did not change significantly with temperature, while the value of B increased with the increase of temperature. The R^2 value obtained by fitting the model fitting was the largest, all above 0.99, and the SSE was relatively small. These results indicated that the adsorption process was a multi-molecular layer adsorption process with uneven surface, and the adsorption was easy to occur. The Langmuir model described the non-ideal monolayer adsorption process, and most of them were chemical adsorption. The adsorption capacities from Langmuir model were 25.5, 24.7, and 24.8 $\text{mg}\cdot\text{g}^{-1}$ at various temperatures, respectively. The difference from Langmuir model and experiments at same temperature was slightly larger, and the SSE was larger, indicating that the process of Fe-SA adsorption of PO_4^{3-} was not a monolayer adsorption. The values of K_F from Freundlich model increased with the increasing of temperature, also indicating that the adsorption of PO_4^{3-} by Fe-SA was endothermic. But the trend of values of $1/n$ was contrast. Although values of R^2 were greater than 0.981, SSE was relatively large, it was not very suitable for Fe-SA to PO_4^{3-} isotherm fitting as the fitted curves were far

from experimental points. The Koble–Corrigan model and Redlich–Peterson model are both three-parameter models. Parameters of g , A , B and n from both models became larger with the increase of temperature while the trend of parameter a from Redlich–Peterson model was opposite. It can be seen from the Table 2 that values of R^2 from both models were larger and values of SSE were also smaller while the fitted curves from both models were closer to experimental points. So both models were as suitable as Temkin model to describe the adsorption behavior of Fe-SA for PO_4^{3-} .

3.2.5. Adsorption kinetic study

The effect of contact time on adsorption at various concentrations and temperature are shown in Fig. 3b–d. It is clearly seen that the adsorption of PO_4^{3-} by Fe-SA was relatively fast in the initial stage, then gradually slowed down, and finally tended to equilibrium. It is also found from Fig. 3b that as the initial concentration of PO_4^{3-} increased, its adsorption capacity gradually increased, but the time required for adsorption to reach equilibrium also increased. Comparing Fig. 3c and d at different temperatures, the same conclusion can be drawn. This might be due to the large difference between the concentration

Table 2
Adsorption isotherm parameters for PO_4^{3-} adsorption on Fe-SA

Langmuir					
T (K)	K_L ($\text{L}\cdot\text{g}^{-1}$)	$q_{e(\text{exp})}$ ($\text{mg}\cdot\text{g}^{-1}$)	$q_{m(\text{theo})}$ ($\text{mg}\cdot\text{g}^{-1}$)	R^2	SSE
293	0.172 ± 0.020	21.3	25.5 ± 0.7	0.978	1.40
303	0.253 ± 0.020	22.0	24.7 ± 0.5	0.976	1.37
313	0.322 ± 0.030	22.4	24.8 ± 0.4	0.980	1.04
Freundlich					
T (K)	$q_{e(\text{exp})}$ ($\text{mg}\cdot\text{g}^{-1}$)	K_F	$1/n$	R^2	SSE
293	21.3	7.48 ± 0.21	0.322 ± 0.010	0.994	0.373
303	22.0	9.34 ± 0.27	0.262 ± 0.011	0.990	0.561
313	22.4	10.6 ± 0.38	0.234 ± 0.013	0.981	1.00
Redlich–Peterson					
T (K)	K	a	g	R^2	SSE
293	15.4 ± 11.0	1.58 ± 1.50	0.746 ± 0.056	0.995	0.285
303	16.2 ± 8.20	1.27 ± 0.86	0.819 ± 0.046	0.993	0.332
313	14.2 ± 5.50	0.883 ± 0.500	0.879 ± 0.051	0.989	0.478
Temkin					
T (K)	A	B		R^2	SSE
293	14.7	30.2		0.994	0.443
303	14.3	33.2		0.992	0.343
313	17.7	35.1		0.993	0.551
Koble–Corrigan					
T (K)	A	B	n	R^2	SSE
293	7.48 ± 0.43	0.146 ± 0.060	0.485 ± 0.11	0.995	0.257
303	10.0 ± 0.6	0.255 ± 0.072	0.485 ± 0.13	0.992	0.366
313	11.6 ± 1.4	0.375 ± 0.038	0.604 ± 0.17	0.988	0.521

Note: $\sum (q - q_c)^2$, q and q_c are the experimental value and calculated value according the model, respectively.

of PO_4^{3-} on the surface of the adsorbent and the solution at high concentrations. The greater the driving force of PO_4^{3-} to transfer resistance between liquid and solid phases, the more relative active sites, and the greater the adsorption capacity is. Therefore, a longer equilibration time was required. With the increase of temperature, the equilibrium adsorption quantity was 18.4, 20.4, 21.6 $\text{mg}\cdot\text{g}^{-1}$ at 293, 303, 313 K ($C_0 = 30 \text{ mg}\cdot\text{L}^{-1}$), respectively. This again confirmed that the process was endothermic.

In this section, non-linear fitting of kinetics data of PO_4^{3-} onto Fe-SA adsorption using the pseudo-first-order kinetic model, pseudo-second-order kinetic model and Elovich equation dynamics model was performed. The fitted curves are also depicted in Fig. 3b–d, and the obtained parameters are shown in Table 3.

It can be seen from Table 3 that the theoretical adsorption amount $q_{e(\text{theo})}$ obtained by the pseudo-second-order kinetic model increased gradually with the increase of temperature and the initial concentration of PO_4^{3-} , and was close to the experimental value $q_{e(\text{exp})}$. The R^2 value was

relatively large and the SSE was small. Moreover, the fitted curves from this model were closer to experimental points. These indicated that the pseudo-second-order kinetic model was suitable to fit the kinetic process and there might be chemical adsorption in the adsorption process. It is seen from Table 3 that values of R^2 from Elovich model were above 0.976 and the SSE was also smaller. So it was referred that Elovich model can be suitable to describe the adsorption process of Fe-SA toward PO_4^{3-} and the adsorption process may contain ion exchange. Compared with the pseudo-second-order kinetic model and Elovich equation, the value of the determined coefficient R^2 fitted by the pseudo-first-order kinetic model was relatively small, and the SSE was large. Furthermore, the fitted curves from this model were not closer to the experimental points. Therefore, it was not suitable to describe the adsorption behavior of Fe-SA toward PO_4^{3-} from solution.

Overall, there is in favor of removal of PO_4^{3-} from solution about Fe-SA at acidic condition, coexisted common salts, higher temperature and higher dose of Fe-SA.

Table 3
Parameters of adsorption kinetics for PO_4^{3-} adsorption on Fe-SA

Pseudo-second-order kinetic model						
T (K)	C_0 (mg·L ⁻¹)	$q_{e(\text{exp})}$ (mg·g ⁻¹)	$q_{e(\text{theo})}$ (mg·g ⁻¹)	$k_2 \times 10^{-4}$	R^2	SSE
293	20	16.5	16.4 ± 0.6	37.8 ± 8.7	0.915	11.4
	30	18.4	19.2 ± 0.6	25.9 ± 4.7	0.955	8.98
	40	20.1	20.9 ± 0.5	22.9 ± 3.3	0.973	6.53
303	20	17.7	19.6 ± 0.6	18.8 ± 3.1	0.971	6.63
	30	20.4	21.2 ± 0.5	22.9 ± 3.3	0.973	6.78
	40	21.9	22.7 ± 0.4	28.3 ± 3.7	0.972	7.24
313	20	18.4	18.6 ± 0.7	29.9 ± 7.1	0.916	14.8
	30	21.6	22.3 ± 0.5	24.6 ± 3.9	0.964	9.59
	40	24.3	25.1 ± 0.4	25.3 ± 2.7	0.983	5.57
Elovich equation						
T (K)	C_0 (mg·L ⁻¹)	$q_{e(\text{exp})}$ (mg·g ⁻¹)	α	β	R^2	SSE
293	20	16.5	3.81	0.368	0.987	1.75
	30	18.4	3.21	0.300	0.985	3.09
	40	20.1	3.17	0.270	0.992	1.88
303	20	17.7	2.25	0.282	0.976	5.43
	30	20.4	3.19	0.267	0.995	1.23
	40	21.9	5.01	0.263	0.991	2.43
313	20	18.4	3.75	0.321	0.987	2.29
	30	21.6	4.15	0.261	0.991	2.34
	40	24.3	5.19	0.234	0.987	4.13
Pseudo-first-order kinetic model						
T (K)	C_0 (mg·L ⁻¹)	$q_{e(\text{exp})}$ (mg·g ⁻¹)	$q_{e(\text{theo})}$ (mg·g ⁻¹)	$k_1 \times 10^{-2}$ (min ⁻¹)	R^2	SSE
293	20	16.5	14.9 ± 0.6	4.20 ± 1.00	0.787	28.4
	30	18.4	17.4 ± 0.6	3.35 ± 0.61	0.880	24.1
	40	20.1	18.9 ± 0.6	3.31 ± 0.54	0.908	22.6
303	20	17.7	17.4 ± 0.5	2.59 ± 0.37	0.934	15.1
	30	20.4	19.0 ± 0.6	3.44 ± 0.58	0.903	24.5
	40	21.9	20.7 ± 0.6	4.52 ± 0.79	0.888	29.2
313	20	18.4	16.9 ± 0.7	3.66 ± 0.85	0.795	36.2
	30	21.6	20.3 ± 0.7	3.72 ± 0.67	0.882	31.0
	40	24.3	22.9 ± 0.6	4.40 ± 0.69	0.912	29.1

3.3. Calculation of thermodynamic parameters and apparent activation energy

According to the formula, the thermodynamic parameters and apparent activation energy of Fe-SA adsorption of PO_4^{3-} were calculated. It was known from the foregoing that the pseudo-second-order kinetic model has a high degree of fitting for Fe-SA adsorption of PO_4^{3-} . Therefore, the rate constant k_2 of the quasi-second-order kinetic model was selected to calculate the apparent activation energy E_a . The results are shown in the Table 4. It can be seen from the table that $\Delta G < 0$, $\Delta H > 0$, and $\Delta S > 0$, indicating that the adsorption reaction was a spontaneous, entropy-increasing endothermic reaction [36].

During the adsorption process, the enthalpy change and activation energy were relatively small, indicating

that the adsorption of Fe-SA to PO_4^{3-} might be physical adsorption. However, in the kinetic analysis, the adsorption of PO_4^{3-} by Fe-SA was more consistent with the pseudo-second-order kinetic model and Elovich model, indicating that there might be a chemical reaction in the adsorption process. In summary, the adsorption of PO_4^{3-} by Fe-SA was a spontaneous adsorption process, and there were both chemical adsorption and physical adsorption during the adsorption process.

3.4. Desorption and regeneration

The process can be made efficient and economical by regeneration of spent adsorbents or recovering adsorbates [37–40]. After adsorption, the spent adsorbent needs to be desorbed or regenerated.

Table 4
Thermodynamic parameters of PO_4^{3-} adsorption onto Fe-SA

E_a (kJ·mol ⁻¹)	ΔH (kJ·mol ⁻¹)	ΔS (J·mol ⁻¹ ·K ⁻¹)	ΔG (kJ·mol ⁻¹)		
			293 K	303 K	313 K
0.530	43.3	11.7	-4.01	-5.08	-5.67

As HCl solution is used, the H^+ ion in the strong acid solution replaced the Fe^{3+} on the material, so the ferric chloride solution is needed for regeneration of Fe-SA. In the three-cycle regeneration experiments, the desorption rates were 80.8%, 76.1%, and 73.3%, respectively, and the regeneration rates were 91.1%, 85.4%, and 82.8% in turn, indicating that Fe-SA was a stable, recyclable, and good adsorbent.

3.5. Adsorption mechanism

According to the experimental results, such as effect of salt concentration, solution pH, the mechanism contain following process: (1) coordination between Fe (existed in Fe-SA) and O (existed in phosphate); (2) hydrogen bond (between $-\text{OH}$ existed in Fe-SA and $-\text{OH}$ existed in phosphate); (3) electrostatic attraction between positive Fe and negative phosphate (not major role).

4. Conclusion

Fe-SA, one stable, green and environmentally friendly adsorbent, was prepared in a simple way. The preparation process was non-toxic, economical and easy to operate. Furthermore, the separation of Fe-SA from mixtures is easily performed using sieve web. The adsorption capacity of SA was improved obviously by Fe modification, and the unit adsorption capacity of PO_4^{3-} was up to 21.3 mg·g⁻¹. The optimum pH value of Fe-SA for PO_4^{3-} adsorption was 3. The presence of coexisting ions had a positive effect on the adsorption of PO_4^{3-} by Fe-SA. The adsorption process of Fe-SA for PO_4^{3-} was consistent with Temkin model, and it was speculated that the adsorption process might be dominated by multi-layer non-uniform surface adsorption. The pseudo-second-order kinetic model can describe the kinetic adsorption behavior of the system well, indicating that chemisorption exists in the adsorption process. The thermodynamic data showed that the adsorption process was spontaneous, entropic and endothermic. The desorption and regeneration study showed that 0.1 mol·L⁻¹ HCl solution had a good desorption effect on PO_4^{3-} -loaded Fe-SA, indicating that the adsorbent had a stable performance and can be recycled. Overall, the Fe-SA here was a promising adsorbent for removal of PO_4^{3-} and had a good application prospect.

Acknowledgements

This work was financially supported by the Henan province basis and advancing technology research project (142300410224).

References

- [1] T.A. Saleh, Protocols for synthesis of nanomaterials, polymers, and green materials as adsorbents for water treatment technologies, *Environ. Technol. Innovation*, 24 (2021) 101821, doi: 10.1016/j.eti.2021.101821.
- [2] F.M. Mpatani, R.P. Han, A.A. Aryee, A.N. Kani, Z.H. Li, L.B. Qu, Adsorption performance of modified agricultural waste materials for removal of emerging micro-contaminant bisphenol A: a comprehensive review, *Sci. Total Environ.*, 780 (2021) 146629, doi: 10.1016/j.scitotenv.2021.146629.
- [3] H.M.S. Munir, N. Feroze, A. Ikhlaq, M. Kazmi, F. Javed, H. Mukhtar, Removal of colour and COD from paper and pulp industry wastewater by ozone and combined ozone/UV process, *Desal. Water Treat.*, 137 (2019) 154–161.
- [4] T.A. Saleh, M. Mustaqeem, M. Khaled, Water treatment technologies in removing heavy metal ions from wastewater: a review, *Environ. Nanotechnol. Monit. Manage.*, 17 (2022) 100617, doi: 10.1016/j.enmm.2021.100617.
- [5] P. Koilraj, K. Sasaki, Selective removal of phosphate using La-porous carbon composites from aqueous solutions: batch and column studies, *Chem. Eng. J.*, 317 (2017) 1059–1068.
- [6] Md. R. Awual, A. Jyo, T. Ihara, N. Seko, M. Tamada, K.T. Lim, Enhanced trace phosphate removal from water by zirconium(IV) loaded fibrous adsorbent, *Water Res.*, 45 (2011) 4592–4600.
- [7] W.Y. Huang, D. Li, Z.Q. Liu, Q. Tao, Y. Zhu, J. Yang, Y.M. Zhang, Kinetics, isotherm, thermodynamic, and adsorption mechanism studies of $\text{La}(\text{OH})_3$ -modified exfoliated vermiculites as highly efficient phosphate adsorbents, *Chem. Eng. J.*, 236 (2014) 191–201.
- [8] M. Lüring, G. Waajen, F. van Oosterhout, Humic substances interfere with phosphate removal by lanthanum modified clay in controlling eutrophication, *Water Res.*, 54 (2014) 78–88.
- [9] R. Howarth, H.W. Paerl, Coastal marine eutrophication: control of both nitrogen and phosphorus is necessary, *Proc. Natl. Acad. Sci. U.S.A.*, 105 (2008) E103, doi: 10.1073/pnas.0807266106.
- [10] Y. Luo, M. Liu, Y. Chen, T. Wang, W. Zhang, Preparation and regeneration of iron-modified nanofibres for low-concentration phosphorus-containing wastewater treatment, *R. Soc. Open Sci.*, 6 (2019) 190764, doi: 10.1098/rsos.190764.
- [11] L. Zhu, Y.Q. Lu, Z.J. He, Preparation and characterization of iron-oxide-coated-zeolite adsorbent, *Adv. Mater. Res.*, 941–944 (2014) 216–220.
- [12] A.A. Aryee, F.M. Mpatani, X. Zhang, A.N. Kani, E. Dovi, R.P. Han, Z.H. Li, L.B. Qu, Iron(III) and iminodiacetic acid functionalized magnetic peanut husk for the removal of phosphate from solution: characterization, kinetic and equilibrium studies, *J. Cleaner Prod.*, 268 (2020) 122191, doi: 10.1016/j.jclepro.2020.122191.
- [13] Y. Shang, X. Xu, S. Qi, Y. Zhao, Z. Ren, B. Gao, Preferable uptake of phosphate by hydrous zirconium oxide nanoparticles embedded in quaternary-ammonium Chinese reed, *J. Colloid Interface Sci.*, 496 (2017) 118–129.
- [14] Q. Liu, P. Hu, J. Wang, L. Zhang, R. Huang, Phosphate adsorption from aqueous solutions by zirconium(IV) loaded cross-linked chitosan particles, *J. Taiwan Inst. Chem. Eng.*, 59 (2016) 311–319.
- [15] K.A. Karimaian, A. Amrane, H. Kazemian, R. Panahi, M. Zarrabi, Retention of phosphorous ions on natural and engineered waste pumice: characterization, equilibrium, competing ions, regeneration, kinetic, equilibrium and thermodynamic study, *Appl. Surf. Sci.*, 284 (2013) 419–431.

- [16] D. Luo, L. Yuan, L. Liu, Y. Wang, W. Fan, The mechanism of biological phosphorus removal under anoxic-aerobic alternation condition with starch as sole carbon source and its biochemical pathway, *Biochem. Eng. J.*, 132 (2018) 90–99.
- [17] K.V. Lo, I. Tunile, H. Tan, T. Burton, T. Kang, A. Srinivasan, P.H. Liao, Microwave enhanced advanced oxidation treatment of sewage sludge from the membrane-enhanced biological phosphorus removal process, *Sep. Purif. Technol.*, 197 (2018) 202–209.
- [18] W. Li, H. Zhang, H. Sun, F. Zeng, Y. Gao, L. Zhu, Influence of pH on short-cut denitrifying phosphorus removal, *Water Sci. Eng.*, 11 (2018) 17–22.
- [19] S. Sun, J. Zhu, Z. Zheng, J. Li, M. Gan, Biosynthesis of β -cyclodextrin modified Schwertmannite and the application in heavy metals adsorption, *Powder Technol.*, 342 (2019) 181–192.
- [20] M. Sharma, J. Singh, S. Hazra, S. Basu, Adsorption of heavy metal ions by mesoporous ZnO and TiO₂@ZnO monoliths: adsorption and kinetic studies, *Microchem. J.*, 145 (2019) 105–112.
- [21] G.Z. Kyzas, G. Bomis, R.I. Kosheleva, E.K. Efthimiadou, E.P. Favvas, M. Kostoglou, A.C. Mitropoulos, Nanobubbles effect on heavy metal ions adsorption by activated carbon, *Chem. Eng. J.*, 356 (2019) 91–97.
- [22] R. Gayathri, K.P. Gopinath, P. Senthil Kumar, S. Suganya, Adsorption capability of surface-modified jujube seeds for Cd(II), Cu(II) and Ni(II) ions removal: mechanism, equilibrium, kinetic and thermodynamic analysis, *Desal. Water Treat.*, 140 (2019) 268–282.
- [23] E. Da'na, Adsorption of heavy metals on functionalized-mesoporous silica: a review, *Microporous Mesoporous Mater.*, 247 (2017) 145–157.
- [24] J. Zhang, M.W. Bligh, P. Liang, T.D. Waite, X. Huang, Phosphorus removal by in situ generated Fe(II): efficacy, kinetics and mechanism, *Water Res.*, 136 (2018) 120–130.
- [25] R. Xue, J. Xu, L. Gu, L. Pan, Q. He, Study of phosphorus removal by using sponge iron adsorption, *Water Air Soil Pollut.*, 229 (2018) 161, doi: 10.1007/s11270-018-3753-x.
- [26] C. Hui, X. Guo, P. Sun, R.A. Khan, Q. Zhang, Y. Liang, Y.-H. Zhao, Removal of nitrite from aqueous solution by *Bacillus amyloliquefaciens* biofilm adsorption, *Bioresour. Technol.*, 248 (2018) 146–152.
- [27] P. Treenate, P. Monvisade, In vitro drug release profiles of pH-sensitive hydroxyethylacryl chitosan/sodium alginate hydrogels using paracetamol as a soluble model drug, *Int. J. Biol. Macromol.*, 99 (2017) 71–78.
- [28] R. Raguvaran, B.K. Manuja, M. Chopra, R. Thakur, T. Anand, A. Kalia, A. Manuja, Sodium alginate and gum acacia hydrogels of ZnO nanoparticles show wound healing effect on fibroblast cells, *Int. J. Biol. Macromol.*, 96 (2017) 185–191.
- [29] C. Peng, J. Zheng, S. Huang, S. Li, D. Li, M. Cheng, Y. Liu, Application of sodium alginate in induced biological soil crusts: enhancing the sand stabilization in the early stage, *J. Appl. Phycol.*, 29 (2017) 1421–1428.
- [30] H. Li, S. Wang, Y. Zhang, L. Chen, High-level expression of a thermally stable alginate Lyase using *Pichia pastoris*: characterization and application in producing brown alginate oligosaccharide, *Mar. Drugs*, 16 (2018) 158, doi: 10.3390/md16050158.
- [31] J.H. Chen, G.P. Li, Q.L. Liu, J.C. Ni, W.B. Wu, J.M. Lin, Cr(III) ionic imprinted polyvinyl alcohol/sodium alginate (PVA/SA) porous composite membranes for selective adsorption of Cr(III) ions, *Chem. Eng. J.*, 165 (2010) 465–473.
- [32] Z.H. Hu, A.M. Omer, X. Ouyang, D. Yu, Fabrication of carboxylated cellulose nanocrystal/sodium alginate hydrogel beads for adsorption of Pb(II) from aqueous solution, *Int. J. Biol. Macromol.*, 108 (2018) 149–157.
- [33] A. Savara, E. Weitz, Elucidation of intermediates and mechanisms in heterogeneous catalysis using infrared spectroscopy, *Annu. Rev. Phys. Chem.*, 65 (2014) 249–273.
- [34] T.A. Saleh, Simultaneous adsorptive desulfurization of diesel fuel over bimetallic nanoparticles loaded on activated carbon, *J. Cleaner Prod.*, 172 (2018) 2123–2132.
- [35] M.A.K.M. Hanafiah, W.S.W. Ngah, S.H. Zolkafly, L.C. Teong, Z.A.A. Majid, Acid Blue 25 adsorption on base treated *Shorea dasyphylla* sawdust: kinetic, isotherm, thermodynamic and spectroscopic analysis, *J. Environ. Sci.*, 24 (2012) 261–268.
- [36] A.A. Aryee, F.M. Mpatani, Y.Y. Du, A.N. Kani, E. Dovi, R.P. Han, Z.H. Li, L.B. Qu, Fe₃O₄ and iminodiacetic acid modified peanut husk as a novel adsorbent for the uptake of Cu(II) and Pb(II) in aqueous solution: characterization, equilibrium and kinetic study, *Environ. Pollut.*, 268 (2021) 115729, doi: 10.1016/j.envpol.2020.115729.
- [37] H.N. Bhatti, Z. Mahmood, A. Kausar, S.M. Yakout, O.H. Shair, M. Iqbal, Biocomposites of polypyrrole, polyaniline and sodium alginate with cellulosic biomass: adsorption–desorption, kinetics and thermodynamic studies for the removal of 2,4-dichlorophenol, *Int. J. Biol. Macromol.*, 153 (2020) 146–157.
- [38] H.M.S. Munir, N. Feroze, N. Feroze, N. Ramzan, M. Sagir, M. Babar, M.S. Tahir, J. Shamshad, M. Mubashir, K.S. Khoo, Fe-zeolite catalyst for ozonation of pulp and paper wastewater for sustainable water resources, *Chemosphere*, 297 (2022) 134032, doi: 10.1016/j.chemosphere.2022.134031.
- [39] S.S. Chen, Z.Y. Zang, S.S. Zhang, G.F. Ouyang, R.P. Han, Preparation of MIL-100(Fe) and multi-walled carbon nanotubes nanocomposite with high adsorption capacity towards oxytetracycline from solution, *J. Environ. Chem. Eng.*, 9 (2021) 104780, doi: 10.1016/j.jece.2020.104780.
- [40] J.L. Wang, X. Liu, M.M. Yang, H.Y. Han, S.S. Zhang, G.F. Ouyang, R.P. Han, Removal of tetracycline using modified wheat straw from solution in batch and column modes, *J. Mol. Liq.*, 338 (2021) 116698, doi: 10.1016/j.molliq.2021.116698.